# 20-kW Bi-directional Wireless Power Transfer System with Energy Storage System Connectivity

Omer C. Onar, Gui-Jia Su, Erdem Asa, Jason Pries, Veda Galigekere, Larry Seiber, Cliff White, Randy Wiles, and Jonathan Wilkins
Power Electronics and Electric Machinery Group, Oak Ridge National Laboratory
National Transportation Research Center, Knoxville, TN 37932, USA
E-mail: onaroc@ornl.gov

*Abstract*— **The severity of the economic impact caused by grid outages has been the driving factor for creating innovative solutions that increases interest for the deployment of distributed energy resources to reduce the impact of grid outages. This study presents a novel way of providing export power using bi-directional wireless power transfer (WPT) systems for ac grid side power and mobile energy storage systems (ESSs) connectivity. The proposed concept here interfaces the EV batteries to the AC grid and also can redirect the power from the stationary ESS to grid, to EV batteries, or both simultaneously; providing the capabilities of an uninterrupted power supply (UPS). Results demonstrate the performance and the functionality of the system with overall efficiencies 93% to 97%, depending on the operating mode.**

***Keywords— bi-directional, grid, energy storage, wireless power transfer, electric vehicle (EV).***

## I. Introduction

Frequent power outages have impacted the reliable power supply to residential / commercial / industrial buildings resulting in reduced comfort and productivity. It has been reported that a two-fold increase in the major power outages has been observed since 2003 [1]. Further increase in such outages can be expected due to the aging grid infrastructure and the observed climate change that leads to frequent occurrence of extreme weather conditions [2]. The economic costs of such outages have been estimated at an average of $100-$200 billion annually [3], [4]. Moreover, hindrance to public safety, online business transaction losses, and other supply chain disturbances have typically not been quantified during power outages [5]. Outages in the distribution system have been much more widespread than the ones in the transmission system, although, the ones in the transmission system cause far greater disruptions. One of the solutions to the power outage problem is the deployment of emergency backup power systems such as portable / standby generators. However, they not only cause pollution and related health problems, but also there are an alarming number of related deaths that have been reported [5] due to these units.

The increased interest in EVs, which include both all-electric and plug-in hybrid electric vehicles, and their higher penetration anticipated in near future leads to the presence of mobile ESSs [6]. These mobile ESSs can not only deliver emergency backup power but also be employed as spinning / non-spinning reserves or regulation providers as source and load and provide ancillary grid services. The aforementioned features in EVs further enhance its marketability through the profits that the customer can make by providing the required grid services. EVs can additionally support the integration of renewable energy resources and/or stationary ESS as shown in Fig. 1. However, the state-of-the-art EVs do not have the capability to transfer power from the vehicle to the grid or provide grid services, typically with the unidirectional ac level-I / II on-board or dc off-board chargers.

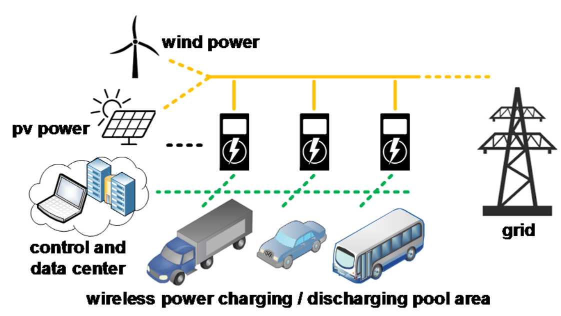


Fig. 1. EVs auxiliary grid service platform.

While bidirectional power transfer is an attractive solution for the above-mentioned problems, there is an inherent problem associated with wired charger system. Especially, during power outages, infrastructure becomes an extremely critical aspect of deploying power to the affected sites. Therefore, it is more difficult to deploy the wired systems as they get bulky as the power increases. Furthermore, they may require a particular type

This manuscript has been authored by Oak Ridge National Laboratory, operated by UT-Battelle, LLC, under Contract No. DE-AC05-00OR22725 with the U.S. Department of Energy. The United States Government retains and the publisher, by accepting the article for publication, acknowledges that the United States Government retains a non-exclusive, paid-up, irrevocable, world-wide license to publish or reproduce the published form of this manuscript, or allow others to do so, for United States Government purposes. The Department of Energy will provide public access to these results of federally sponsored research in accordance with the DOE Public Access Plan (http://energy.gov/downloads/doe-public-access-plan).

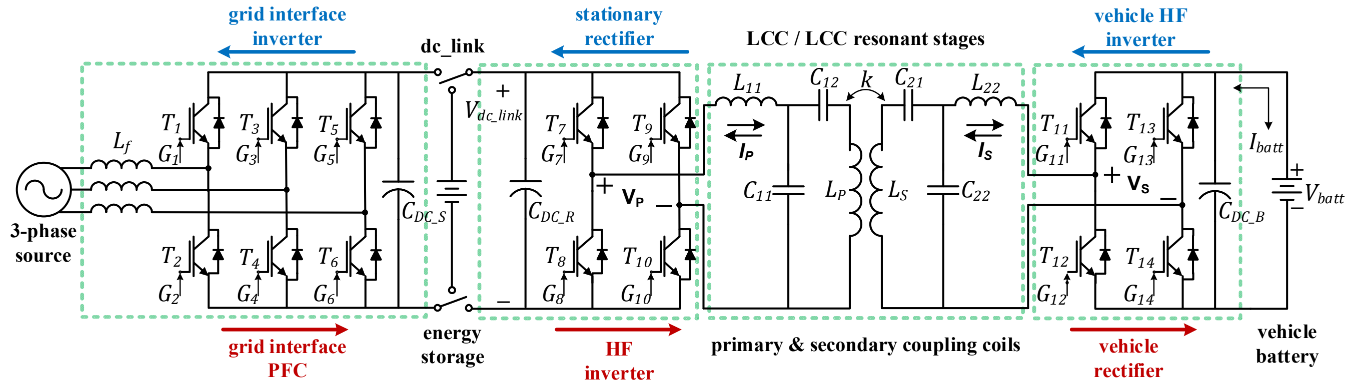


Fig. 2. The proposed high-power bi-directional wireless EV battery charging model with energy storage and grid inteface.

of connector or a plug system that may not be available at the time of deployment. WPT technology offers flexibility and the inherent galvanic isolation which are the two critical components for use in harsh environments and inclement weather conditions for emergency power systems [7]-[8]. Although unidirectional wireless systems research has been growing at a rapid rate in the past few years, only a few research groups have worked on the bi-directional aspect. Moreover, the research work presented so far has been on systems that are less than a few kilowatts. This study presents a 20-kW bi-directional WPT with multiple interfaces for energy storage and grid applications with experimental validation of the system.

## II. The Proposed Bi-directional Wireless Power Transfer System Architecture

The proposed bi-directional wireless charging architecture is shown in Fig. 2. This system allows transferring power from grid to the vehicle battery. Furthermore, this architecture can discharge the vehicle battery wirelessly to the ac grid or to the primary-side dc bus where a battery energy storage system can be connected. The energy storage system connected to the primary-side dc bus can also provide power back to the grid or it can be used to charge the vehicle battery. This functionality might be particularly useful for time of use energy cost management applications. For instance, the stationary energy storage system can be charged from the grid when the consumption is relatively low and electricity prices are low; then, the vehicle can be charged in the evening using the energy previously stored in the stationary energy storage system in order to offset the demand of the vehicle charging. The stationary ESS can also be used during emergencies as a backup power source. In case the vehicle needs to be charged during grid outages, the energy stored in the ESS can be used.

As presented in Fig. 2, the system consists of a three-phase ac/dc converter with power factor correction (PFC), a high-frequency H-bridge inverter, resonant network with WPT couplers and resonant tuning circuitry, and the vehicle-side rectifier and filter during charging. The grid interface converter becomes a three-phase inverter, primary-side H-bridge inverter becomes a rectifier, and vehicle-side rectifier becomes an inverter when discharging the vehicle battery back to the grid. The stationary ESS can either source or sink the power in both power flow directions. The resonant stage used in this system is an *LCC* / *LCC* combination of the passive inductor and capacitor components, where the primary side $L_{11}$, $C_{11}$, $C_{12}$, $L_P$ and the secondary $L_S$, $C_{22}$, $C_{21}$, $L_{21}$ values are given in Table I.

TABLE I. System Parameters.

| Parameter | Value |
|---|---|
| $L_{11}$ | 52.1 µH |
| $C_{11}$ | 1.0 µF |
| $C_{12}$ | 0.67 µF |
| $L_P$ | 129.95 µH |
| $k$ | 0.21 |
| $L_S$ | 125.4 µH |
| $C_{21}$ | 0.57 µF |
| $C_{22}$ | 1.33 µF |
| $L_{22}$ | 37.6 µH |

The equivalent circuit diagram of the resonant stage with WPT coupling coils and resonant tuning components is shown in Fig. 3.

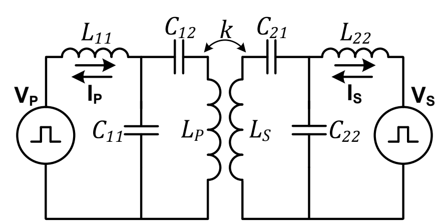

Fig. 3. LCC / LCC resonat stage of wireless power link.

WPT coils with primary and secondary inductances $L_P$, $L_S$, and coupling coefficient of $k$ can be modeled as a coupled inductor with magnetizing inductance as

$$L_M = k\sqrt{L_P L_S} \quad (1)$$

and leakage inductances of the primary coil $L_{l,p}$ and secondary coil $L_{l,s}$ can be defined as

$$L_{l,p} = L_P - L_M \quad (2)$$

$$L_{l,s} = L_S - L_M \quad (3)$$

The load resistance at the output of the secondary side tuning network can be described as

$$R_{L,batt} = \frac{8}{\pi^2}\frac{V_{batt}^2}{P_{batt}} \quad (4)$$

and equivalent ac resistance at the input of the resonant tank can be defined as

$$R_{L,dc\_link} = \frac{8}{\pi^2}\frac{V_{dc\_link}^2}{P_{dc\_link}} \quad (5)$$

Using the Kirchhoff's law, primary and secondary resonant network in a matrix form can be expressed by

$$\begin{bmatrix} V_{dc\_link} \\ V_{batt} \end{bmatrix} = \begin{bmatrix} \left(j\omega L_{11} // \frac{1}{j\omega C_{11}}\right) + \frac{1}{j\omega C_{12}} + j\omega L_{l,p} + j\omega L_M & -j\omega L_M \\ -j\omega L_M & \frac{1}{n^2}\left(j\omega L_{22} // \frac{1}{j\omega C_{22}}\right) + \frac{1}{n^2 j\omega C_{21}} + \frac{j\omega L_{l,s}}{n^2} + j\omega L_M \end{bmatrix} \begin{bmatrix} I_{dc\_link} \\ I_{batt} \end{bmatrix} \quad (6)$$

where $n$ is the turns ratio between primary and secondary coils which is defined by $n = \sqrt{L_S/L_P}$. If the system components satisfy resonant frequency compensation requirements $\omega_o$ as

$$\omega_o = 1/\sqrt{L_{11}C_{11}} = 1/\sqrt{L_{22}C_{22}} \quad (7)$$

and

$$\omega_o = 1/\sqrt{(L_P - L_{11})C_{12}} = 1/\sqrt{(L_S - L_{22})C_{21}} \quad (8)$$

The corresponding voltage transfer functions of the bi-directional system in charging mode can be expressed by

$$\left|M_{V,charge}\right| = \left|\frac{V_{batt}}{V_{dc\_link}}\right| = \left|\frac{\omega^2 L_M C_{11}}{(1-(\omega/\omega_o)^2 + j\omega C_{22}R_{L,batt})(1/C_{21} + j\omega L_S) + j\omega L_{22} + R_{L,dc\_link}}\right| \quad (9)$$

and during discharge mode by

$$\left|M_{V,discharge}\right| = \left|\frac{V_{dc\_link}}{V_{batt}}\right| = \left|\frac{\omega^2 L_M C_{22}}{(1-(\omega/\omega_o)^2 + j\omega C_{11}R_{L,dc\_link})(1/C_{12} + j\omega L_P) + j\omega L_{11} + R_{L,batt}}\right| \quad (10)$$

The proposed system gain margin is designed differently for input and output voltage amplitudes over the operating frequency range of the bi-directional operation. The grid rectified input dc link voltage ranges from 680 V to 800 V while the vehicle battery voltage ranges from 310 V to 430 V with 420 V being the nominal voltage. The nominal voltage of the input dc link and battery are considered 800 V and 350 V, respectively. Therefore, at the rated power of 20 kW, the grid to vehicle (G2V) system operates in step-down mode with a nominal gain of 0.43 and the vehicle to grid (V2G) operates in boost mode with a nominal voltage gain of 2.2. The grid to vehicle voltage gain $|M_{V,charge}|$ and vehicle to grid voltage gain $|M_{V,discharge}|$ variations with respect to load and the switching frequency are presented in Fig. 4. The frequency response results show that both the gain margins charge, and discharge are highly sensitive to the frequency around the resonant frequency of 22 kHz. Some additional characteristics of the double-sided *LCC* tuning topology can be found in [9] and [10] while the resonant gain characteristics of this proposed system is investigated in [11] along with the sensitivity analysis.

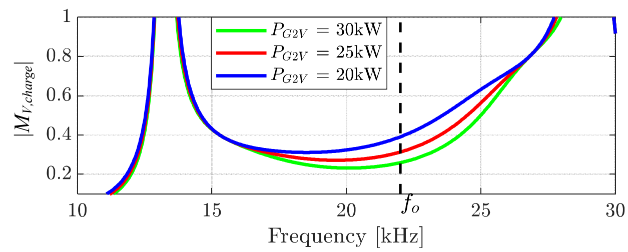


(a)

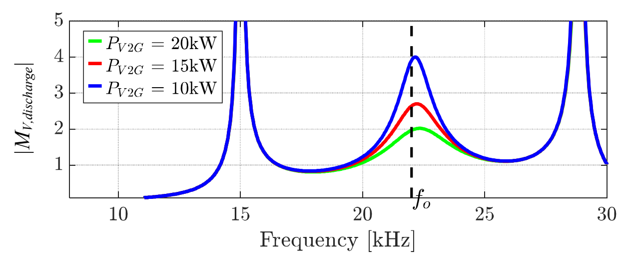


(b)

Fig. 4. The proposed system voltage gain margin for (a) grid to vehicle (G2V) $|M_{V,charge}|$ and (b) vehicle to grid (V2G) $|M_{V,discharge}|$.

## III. The System Simulation Analysis

During charging mode (G2V), the system control is established on the dc link voltage that manages the vehicle battery current from the dc link; i.e., higher primary-side dc bus voltage results in higher battery current. In reversed power flow operation (V2G), the vehicle side converter is operated in inverter mode, powering the vehicle-side coil. The induced voltage in stationary side coil steps-up the voltage through resonant compensation, then the stationary-side resonant inverter applies dc voltage to the input of the grid side inverter to generate 480 V 60 Hz 3-phase voltage. The simulation results of the proposed system for G2V and V2G operating modes are presented in Figs. 5 and 6, respectively. As seen from the closed loop simulation results, the power factor of the system is around 0.99 and grid current THD level is less than 2% for both conditions G2V and V2G. Estimated efficiency is around 92% from grid to the battery or battery to the grid.

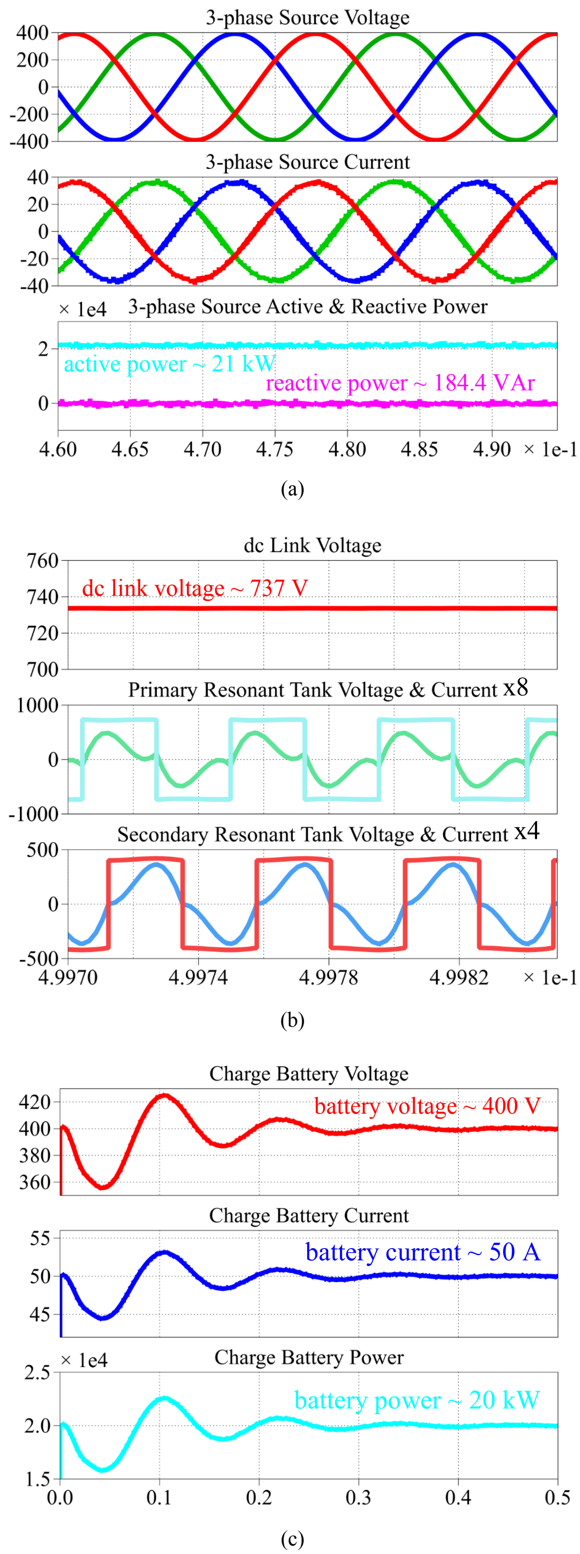


Fig. 5. Simulation results of the system from G2V at full power, (a) grid side voltage, current, and active / reactive power, (b) dc link voltage, primary / secondary resonant tank voltage, and current, (c) the battery voltage, current, and power waveforms.

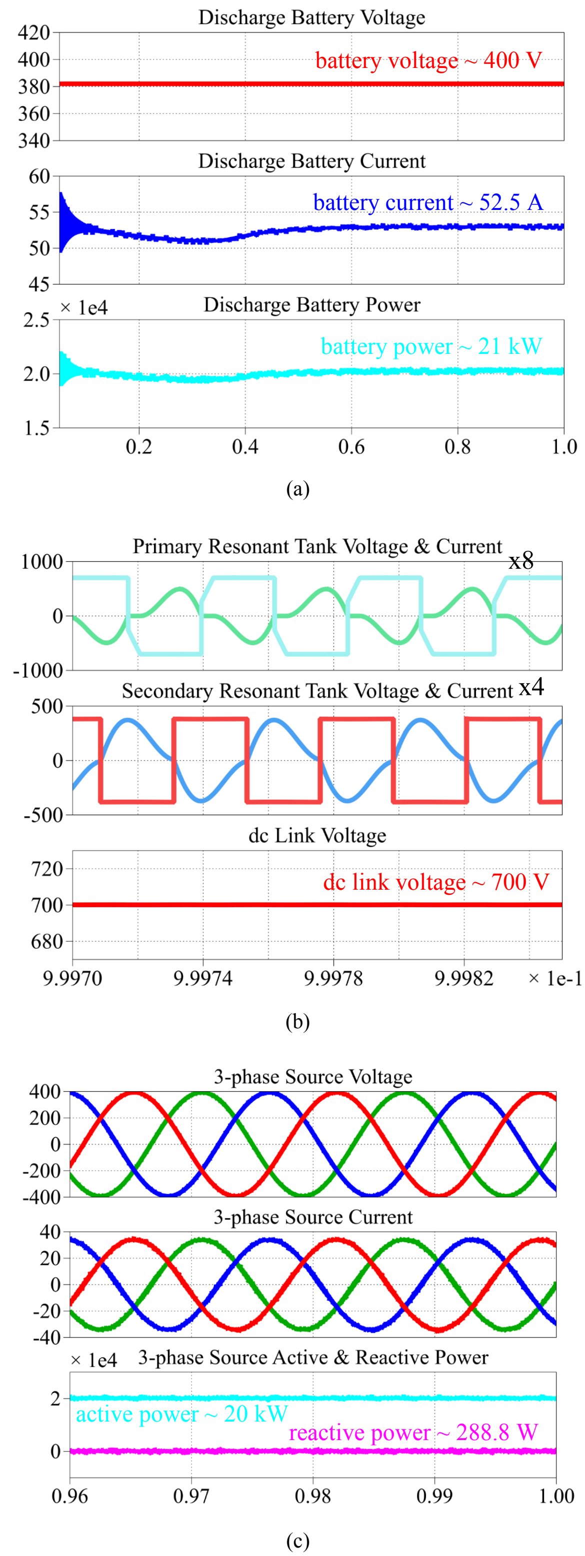


Fig. 6. Simulation results of the system from V2G at full power, (a) the battery voltage, current, and power, (b) dc link voltage, primary / secondary resonant tank voltage and current, (c) grid side voltage, current, and active / reactive power waveforms.

## IV. Experimental Results

A test setup was built in authors' laboratory for experimental verifications and demonstrating the operation of the bi-directional WPT system with grid integration and ESSs. The hardware developed for primary and secondary sides as well as the primary and secondary coils with 11 inches of magnetic airgap separation are shown in Fig. 7.

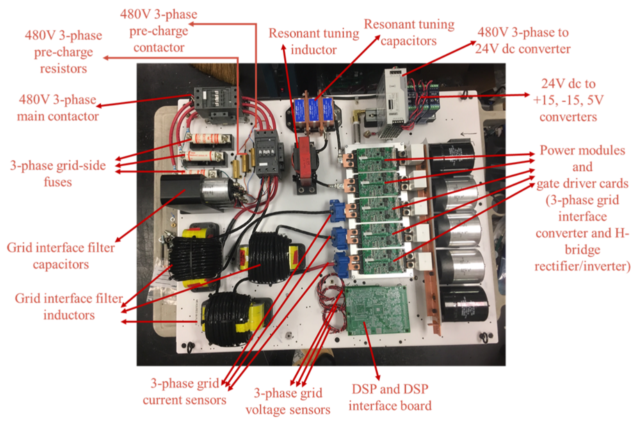


(a)

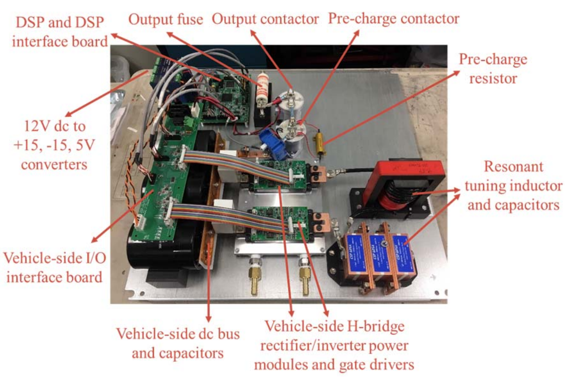


(b)

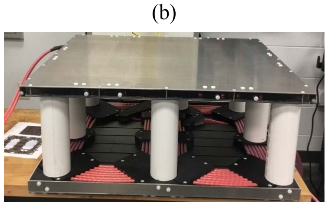

(c)

Fig. 7. Hardware development for the bidirectional WPT system: (a) primary-side grid interface converter, H-bridge inverter/rectifier, and resonant tuning components, (b) secondary-side H-bridge rectifier/inverter and resonant tuning components, and (c) coupling coils.

As shown in Fig. 7 (a), there are five power modules utilized in the primary-side hardware including three modules to form the 3-phase grid interface converter and an H-bridge inverter / rectifier with two power modules; all sharing the same dc bus. Power modules are the 1200 V / 300 A rated dual ROHM SiC phase-leg devices. Both primary and secondary-side power modules are cooled with a liquid cooling system using water and ethylene glycol mix on Microcool cold plates. The control systems of the primary and secondary sides are implemented using a TMS320F28377DPTPS DSP module from Texas Instruments. Additional system parameters are provided in Table II.

Table II. Experimental System Parameters.

| Parameter | Value |
|---|---|
| 3-phase grid voltage | 480 $V_{AC}$ |
| Nominal G2V / V2G power | 20 kW |
| Primary dc link voltage range | 675 V - 800 V |
| Vehicle battery voltage range | 310 V - 400 V |
| Stationary ESS voltage rage | 700-800V |
| Magnetic air gap | 11 inches |
| Coil dimensions | 34x28.5x1.5 inches |
| Resonance frequency | 22.0 kHz |

In G2V experiments, and NHR 9400 grid simulator was used in constant voltage mode, set to 480 V, 60 Hz 3-phase to emulate the power grid while NHR 9300 battery emulator was used to emulate the vehicle battery.

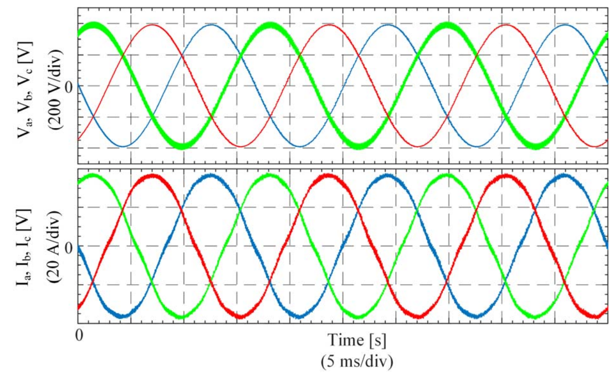


(a)

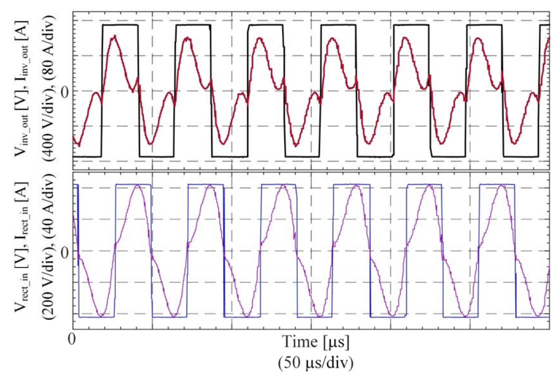


(b)

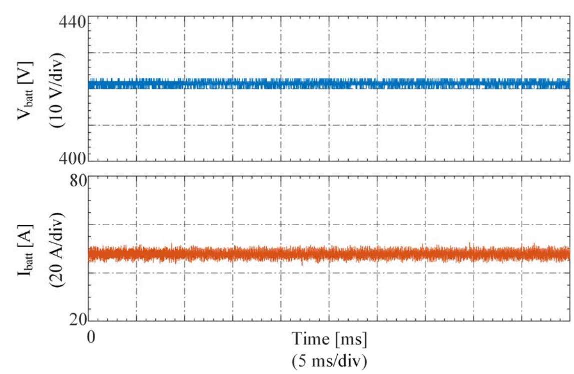


(c)

Fig. 8. Experimental results: (a) Grid-side 3-phase voltages and currents, (b) primary inverter output voltage and current and secondary rectifier input voltage and current (~22 kHz), and vehicle-side battery voltage and current.

In Fig. 8, experimental test results of the G2V operation is shown where Fig. 8 (a) shows the grid voltage and current, Fig. 8 (b) shows the primary-side H-bridge inverter output voltage and current and secondary-side rectifier input voltage and current, and Fig. 8 (c) shows the vehicle-side battery voltage and current. In Fig. 9, the Yokogawa WT1800 power analyzer screenshot is provided to display the stage-by-stage power flow and all of the power conversion efficiencies.

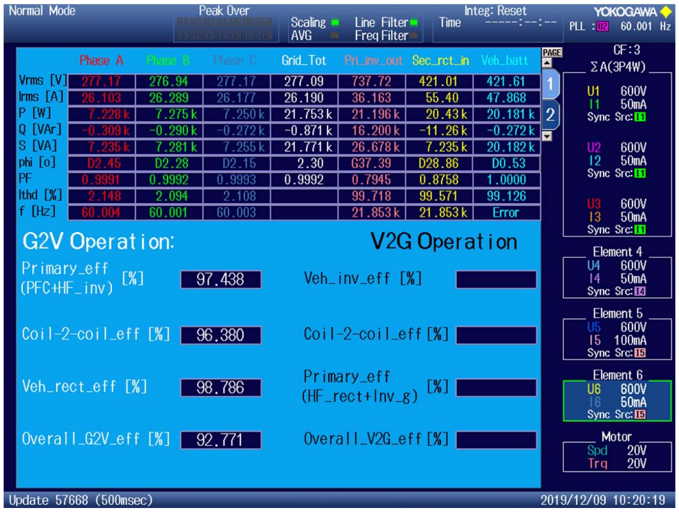


Fig. 9. Experimental results for G2V operation with state-by-stage power flow and efficiencies.

In Fig. 9, phase A, B, and C on the first three columns indicate the readings from the 3-phase grid connection. As seen from the figure, the power factor on the grid interface is 0.99 on all phases and the total harmonic distortion (THD) on grid current is about 2.1% on all phases. Typically, the requirement for power factor is >0.9 while the requirement for THD is <5%. In total, there is 21.75 kW power delivered from grid to the system. Primary inverter output power is 21.19 kW which indicates a combined efficiency of primary side is 97.44% (including the efficiency of the PFC rectifier and the H-bridge inverter). Coil-to-coil efficiency is measured 96.38% across 11 inches airgap and this efficiency takes the losses of the primary and secondary resonant tuning components (*LCC* / *LCC*) into account. Finally, vehicle rectifier operates at 98.78% efficiency. The overall end-to-end efficiency is then 92.77% all the way from 3-phase grid to the battery terminals.

Next, the performance and functionality of the system is tested with the stationary ESS connected to the primary-side dc bus. In this mode of operation, in order to simultaneously test the grid interface converter and dc-to-dc vehicle battery charging, grid interface converter is operated in 3-phase inverter mode, providing power back to the grid (or building loads), while the primary-side H-bridge is also operated in inverter mode, delivering power to the primary coil and the resonant stage. The stationary ESS voltage on the battery emulator is set to 758V. The grid-interface inverter is controlled to inject about 31A to the grid which resulted in about 23.65 kW power delivery from ESS to the utility grid. At the same time, an additional 20.41 kW is processed by the H-bridge inverter to charge the vehicle. In total, stationary ESS provides 44.61 kW to the primary-side dc bus of which a portion is directed to the vehicle charging and the other portion is used to provide power back to the grid. The power analyzer screenshot for this operating mode is provided in Fig. 10 (a). In Fig. 10 (b) the operational waveforms are presented. In this figure, Element-1, 2, and 3 correspond to the phases A, B, and C on the grid connection while ΣA(3P4W) indicates the total grid readings, Element-5 is the measurements for the stationary ESS, and Element-6 is the primary-side H-bridge inverter output. According to the power measurements, the primary-side combined efficiency can be calculated as

$$\eta = \frac{20.414+23.650}{44.613}100 = 98.77\%. \qquad (11)$$

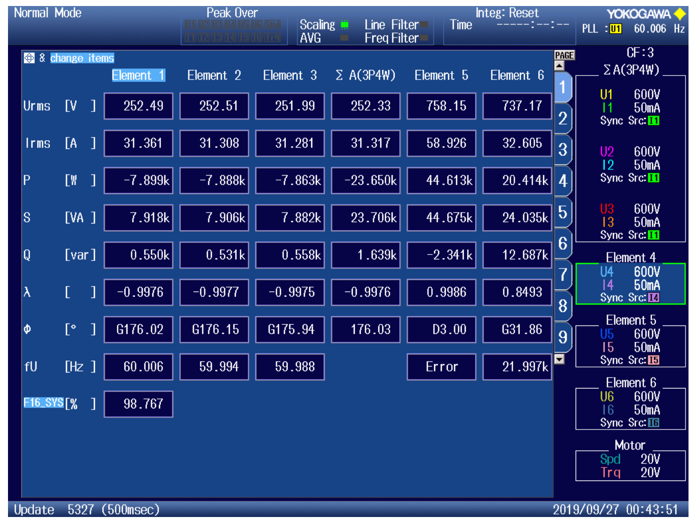


(a)

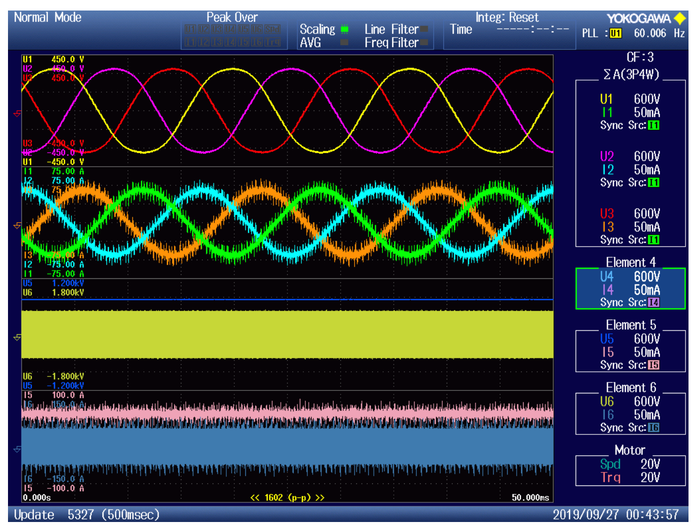


(b)

Fig. 10. Experimental results for simultaneous testing the functionality of providing power back to the grid and charging the vehicle: (a) Numerical measurements and (b) waveforms.

## V. Conclusions

This study introduces a bi-directional wireless power transfer system with double-sided *LCC* resonant tuning with 11 inches of airgap separation between the coils. The proposed system also features a stationary ESS that can be connected at the primary-side dc bus. In this configuration, vehicle can charge both the stationary ESS and the vehicle battery while the ESS can also independently charge the vehicle battery during grid outages. Moreover, ESS can provide power back to the grid or local loads while wirelessly charging the vehicle battery. With these functionalities, the proposed system can be used as an emergency backup power system or to provide grid support services and demand response. Also, proposed system can be utilized for peak shaving or time of use energy cost management applications. Theoretical analysis, modeling and simulation of the proposed system is presented in this study along with the experimental verifications for two of the prominent operating modes. According to the experimental results, vehicle battery can be charged with 20 kW power at 92.7% overall grid-to-vehicle battery efficiency. At the same time, the ESS can provide power back to the grid and vehicle battery with a combined primary-side efficiency of 98.76% with a total of 44.61 kW power out of the stationary ESS.

## REFERENCES


[1] A. Kenward and U. Raja, "Blackout: Extreme weather, climate change, and power outages" *Climate Central*, 2014.

[2] R. J. Campbell, "Weather-related power outages and electric system resiliency" *Congressional Research Service*, 2012.

[3] LaCommare, K. Hamachi and J. H. Eto, "Cost of power interruptions to electricity consumers in the United States," *Energy*, 2005.

[4] Primen, "The Cost of power disturbances to industrial and digital economy companies," *TR-1006274*, 2001.

[5] "Economic benefits of increasing electric grid resilience to weather outages" *Executive Office of the President*, 2013.

[6] S. Shepard and J. Gartner, "Vehicle to grid technologies," *Navigant Research*, 2013.

[7] E. Asa, K. Colak, D. Czarkowski, B. Tamyurek, "Efficiency analysis of a Bi-directional DC / DC converter for wireless energy transfer applications," IEEE Energy Conversion Congress and Exposition (ECCE'15), Montreal, QC, 2015, pp. 594-598.

[8] K. Colak, E. Asa, D. Czarkowski, H. Komurcugil, "A novel multi-level bi-directional DC / DC converter for inductive power transfer applications," 41st Annual Conference of the IEEE Industrial Electronics Society (IECON'15), Yokohama, 2015, pp. 3827-3831.

[9] H. Chu, X. Qu, S. -C. Wong, and C. K. Tse, "Design of an IPT battery charger with double-sided LCC compensation," IEEE Energy Conversion Congress and Exposition (ECCE'18), pp. 1184-1189, September 2018, Portland, OR.

[10] S. Zou, O. C. Onar, V. Galigekere, J. Pries, G. -J. Su, and A. Khaligh, "Secondary active rectifier control scheme for a wirelesss power transfer system with double-sided LCC compensation topology," 44th Annual Conference of the IEEE Industrial Electronics Society (IECON'18), pp. 2145-2150, October 2018, Washington, D.C.

[11] M. Mohammad, S. Anwar, O. Onar, J. Pries, V. Galigekere, E. Asa, G. -J. Su, and J. Wilkins, "Sensitivity analysis of an LCC-LCC compensated 20-kW bidirectional wireless charging system for medium-duty vehicles," IEEE Transportation Electrification Conference and Expo (ITEC'19), pp. 1-7, June 2019, Detroit, MI.